Adsorption 8: 147–155, 2002

Air Separation by Carbon Molecular Sieves

A.I. SHIRLEY AND N.O. LEMCOFF*
The BOC Group, 100 Mountain Avenue, Murray Hill, NJ 07974, USA

Received August 15, 2001; Revised February 1, 2002; Accepted February 11, 2002

Abstract. The separation of nitrogen from air on a carbon molecular sieve is achieved by a difference in the adsorption kinetics of oxygen and nitrogen. Assuming the oxygen is adsorbed under equilibrium conditions, a simplified analysis is developed for determining the process performance. As expected, a good agreement is observed between the simplified and full analysis for long cycle times, but for short cycle times, neglecting the oxygen adsorption kinetics leads to erroneous purity predictions. Also, the effect of the adsorption/desorption rate constants on the performance of the pressure swing adsorption process is analyzed, and it is found to be a function of the adsorption/desorption step length. Good agreement between the numerical simulation and experimental results is observed over a wide range of product purities.

Keywords: carbon molecular sieve, pressure swing adsorption, separation, nitrogen, air

Introduction

Pressure swing adsorption is widely used in the separation of air to produce oxygen and nitrogen in small to medium size plants. Zeolites, which preferentially adsorb nitrogen, are used for the production of oxygen, while for the production of nitrogen, carbon molecular sieves (CMS) are the preferred adsorbents (Yang, 1987; Ruthven et al., 1994; LaCava and Lemcoff, 1997). The CMS does not show a significant difference in equilibrium adsorption capacities between oxygen and nitrogen. However, oxygen is adsorbed faster than nitrogen, leading to a kinetic selectivity, which allows achieving nitrogen purities as high as 99.999%. The transport process controlling the uptake rate of a gas seems to obey two different mechanisms, either diffusional molecular transport within the bulk of the micropores—Fickian sieves—or surface barrier at the micropore entrances—non-Fickian sieves (Lemcoff, 1999). Different equations have been proposed in the literature to describe the uptake of oxygen and nitrogen. While the linear driving force model is used to approximate the diffusion controlled rates in Fickian sieves, to get a good representation of the actual process in non-Fickian sieves, either a Langmuir type or a slit potential equation have been used. The process performance can then be estimated from the numerical solution of the differential equations. Models presented in the literature have been validated through comparisons with experimental results, and allow predicting the effect of the different process variables. Raghavan and Ruthven (1985) analyzed the effect of feed time on process performance, and found that, at a constant feed flowrate, the yield increases with cycle time while the oxygen concentration goes through a minimum. On the other hand, at constant product purity, both productivity and yield go through a maximum (Lemcoff, 1999). Recently, LaCava and Lemcoff (1996) and Shirley and Lemcoff (1997) studied both experimentally and theoretically the nitrogen pressure swing adsorption process in the high purity region, and found that the effect of cycle time on the process performance becomes more significant as the purity increases. When operating on a long cycle time, oxygen adsorption can be considered to have reached equilibrium throughout most of the bed. In this situation, only the nitrogen kinetic equation has to be considered, and a simplified analysis can be carried out. The validity of this assumption will be examined

*To whom correspondence should be addressed.

in this paper as a function of the process operating conditions.

Previous studies have also shown that, while a change in the oxygen uptake rate affects mainly the purity, a change in the nitrogen uptake rate affects mainly the recovery (Ruthven and Farooq, 1990; Farooq and Ruthven, 1991). It was also observed that, at constant kinetic selectivity, the productivity increases with the uptake rate, while the effect on the yield depends on whether a constant or variable cycle time is assumed (Schork et al., 1993). However, as will be shown in this paper, the product purity can significantly affect this behavior. The effect of the adsorption rate constants on the performance of the pressure swing adsorption process will be studied at different cycle times and product flowrates (nitrogen purities). A comparison between numerical simulation and experimental results will also be presented.

Theoretical Model

The nitrogen PSA unit is assumed to operate on a four-step cycle. In the first step, one bed is pressurized with air, cocurrently producing nitrogen gas, while the second bed is regenerated by a countercurrent purge with product gas at atmospheric pressure. At the end of this first step, the beds are brought into fluid communication, causing gases from the bed at high pressure to flow into the regenerated bed until pressure equalization occurs. A countercurrent blowdown step allows the first bed to vent to the atmosphere, and it is followed by the regeneration of the low-pressure bed, which is purged with a small fraction of the purified product stream.

The following assumptions were made in the model development:

- The system is non-isothermal and the flow pattern is described by the axial dispersion model.
- The pressure is assumed to increase linearly during pressurization, and follow an exponential decay during blowdown. In the equalization step, the detailed composition profile for the pressurizing gas is taken from the corresponding profile of the depressurizing gas of the other bed (point by point model).
- The uptake rate of gases by the non-Fickian carbon molecular sieves used in the present work is described in terms of the slit-potential rate model. Carbon molecular sieves contain small carbon crystallites that are loosely cross-linked with other crystallites to form an aperture cavity structure. The aperture has a slit shape, which serves as an entrance to the cavity formed by several crystallites. Therefore, the adsorption process consists in two consecutive steps, namely crossing the activation energy barrier at the entrance of the slit, and adsorption on the cavity surface following the classical Langmuir adsorption rate. The overall adsorption rate can be described by (LaCava et al., 1989b):

$$R_i = \frac{\partial q_i}{\partial t} = \frac{k_{sli} q_{mi}}{K_i(1-\theta_i)}[K_i c_i(1-\Sigma\theta_k)-\theta_i] \quad (1)$$

In the limit of very high coverage or when the slit potential does not control the rate, Eq. (1) reduces to the classical Langmuir form.

$$R_i = \frac{\partial q_i}{\partial t} = k_{di} q_{mi}[K_i c_i(1-\Sigma\theta_k)-\theta_i] \quad (2)$$

The mass and heat balance equations are described in detail elsewhere (Lemcoff, 1999).

A characteristic of the non-Fickian sieves is that the adsorption half-time depends on the equilibrium coverage. For microbalance measurements with a non-Fickian sieve that follows Langmuir rate model, the adsorption half-time can be expressed as:

$$t_{i^{1/2}} = \frac{0.6931(1-\theta_{ei})}{k_{di}} \quad (3)$$

where $1-\theta_{ei} = \frac{1}{1+K_i C_i}$.

In a multicomponent system, the half-time is also a function of the adsorption properties and concentrations of the other components in the mixture.

When one of the components in the feed gas is adsorbed at a fast rate compared with the production time, a simplification can be introduced. Instead of using the rate equation, the amount adsorbed can be determined directly from the adsorption equilibrium constant. In the present case, the oxygen can be considered to satisfy this condition.

Numerical simulations were carried out using the Dynamic Adsorption Process Simulator—DAPS (LaCava et al., 1989a). The numerical integration of the partial differential equations is carried out by using the method of lines. Finite differences are used in the spatial discretization procedure, and the Adams multistep method as the time integrator.

Adsorption kinetic and equilibrium data was measured independently. The oxygen and nitrogen monolayer capacities were determined to be 1.8 mole/kg,

and the heat of adsorption for nitrogen and oxygen are −16.3 kJ/mol and −14.1 kJ/mol, respectively. The nitrogen and oxygen adsorption half-times at 25°C are 490 s and 21 s, respectively, and the corresponding activation energies for desorption are 31.8 kJ/mol, and 14.5 kJ/mol, respectively.

Experimental Part

The experiments were carried in a commercial scale two-bed nitrogen PSA unit, operating on a four-step cycle, as described above. Tests were carried out at full cycle times between 120 and 1200 s, product flowrates between 25 and 120 Nm^3/h (0°C, 1 atm), and adsorption pressures between 6.5 and 9.0 atm (6.6×10^5 and 9.1×10^5 Pa). The change in the cycle time was achieved by changing simultaneously the duration of the production and purge steps from 46 s to 586 s. The duration of the remaining steps, namely pressurization (10 s), blowdown (10 s), and equalization (4 s), were not modified.

Results and Discussion

To analyze the assumption of equilibrium conditions for oxygen, two different approaches were used. In the first approach, the numerical solution of the differential equations was carried out under the assumption of equilibrium adsorption for oxygen. In the second approach, a finite oxygen adsorption rate was initially assumed, and again the differential mass and heat balance equations were solved. Then, the oxygen adsorption rate was increased until an asymptotic solution was achieved. Both the adsorption and desorption rate constants for nitrogen, and the oxygen adsorption equilibrium constant (ratio of adsorption and desorption rate constants) were kept the same as in the base case. As expected, the predicted performance from the first approach is coincident with the values calculated according to the second approach, for the very fast oxygen adsorption/desorption rates.

When using the rate equations for both components, the computational time per iteration increases with the oxygen adsorption rate. For example, for a ten-fold increase in the adsorption rate constant, the computation time increases between 3 and 10 times. As the system approaches equilibrium conditions, the computational time may become prohibitive. On the other hand, when equilibrium was assumed for oxygen, the computational time per iteration remains relatively low.

The effect of the oxygen adsorption rate on the N_2 PSA performance is represented in Figs. 1 and 2. While the nitrogen yield is almost independent of the oxygen adsorption rate, the nitrogen purity varies significantly. This variation is a strong function of the production time. At short cycle times, the amount of oxygen entering the bed during the feed step is small compared

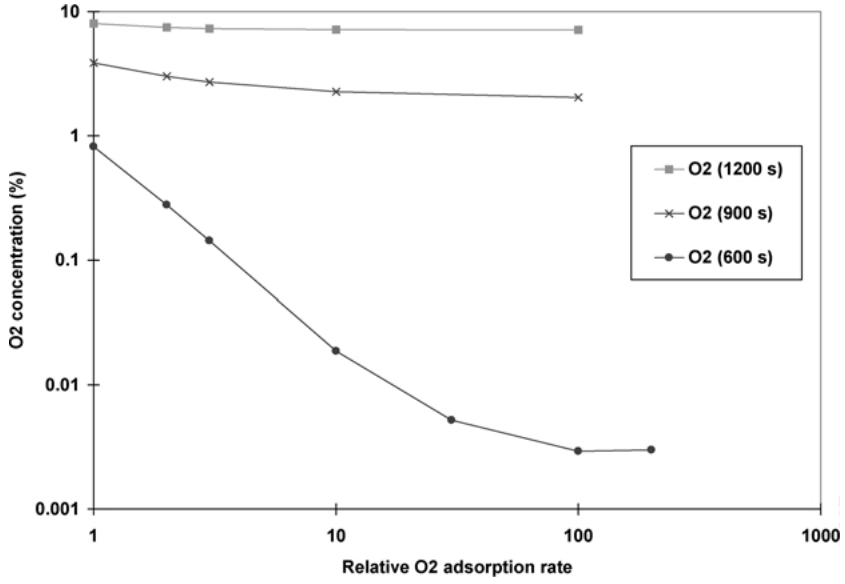

Figure 1. Effect of oxygen adsorption/desorption kinetics on product purity $P = 7.9 \times 10^5$ Pa, product flow = 35 Nm^3/h, $T = 298$ K.

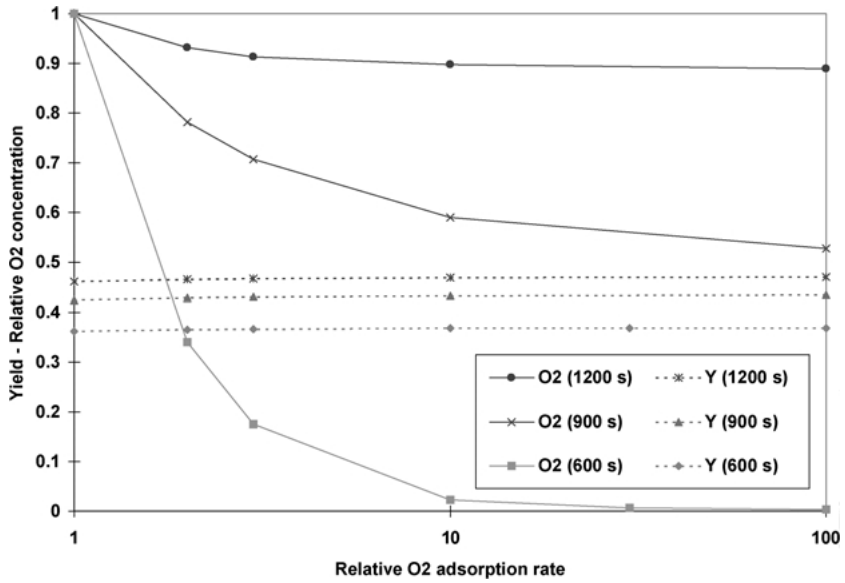

Figure 2. Effect of oxygen adsorption/desorption kinetics on the N_2 PSA performance. $P = 7.9 \times 10^5$ Pa, product flow $= 35$ Nm^3/h, $T = 298$ K.

with the adsorption capacity of the adsorbent. The system is far from the equilibrium conditions, and the adsorption/desorption rate has a significant effect on the performance. On the other hand, for long cycle times, the system is close to equilibrium conditions, and the oxygen adsorption rate has a much smaller effect. In this case, only a small variation in nitrogen purity is observed for a two orders of magnitude change in the oxygen adsorption rate.

It can also be seen that, at constant product flow, both yield and oxygen concentration increase with feed time. However, the dependence of yield on the cycle time is less than linear, and the total feed volume per step also increases with cycle time. For very long cycle times, an asymptotic value should be achieved, which corresponds to the point when the whole bed is saturated with oxygen.

In order to get a better understanding of the effect of productivity and cycle time, and to establish a criterion for the applicability of the oxygen equilibrium assumption, further analysis of the results was carried out. The oxygen concentration in the product is plotted, for different product flowrates, as a function of a normalized cycle time (Fig. 3). The normalized cycle time is defined as $\mathrm{CT} * (F/F_o)$, where CT is the full cycle time, and F, the feed flowrate. A reference value of the feed, $F_o = 126$ Nm^3/h, is used to keep the time dimensions. Since the product $\mathrm{CT} * F$ represents the amount of feed gas that enters the bed during one cycle, a single relationship should exist, except for short cycle times, between the purity and the normalized cycle time. It can be seen that the results for kinetic and equilibrium conditions tend to group themselves along two characteristic curves. Although they differ at short cycle times (medium to high purities), they converge to the same curve at long cycle times (low purities). Thus, for a product flowrate of 35 Nm^3/h, the results for kinetic and equilibrium conditions differ by less than 5% for cycle times greater than 1400 s. This critical cycle time is also found to be a function of the kinetic selectivity. As the selectivity doubles, the critical cycle time decreases to 1200 s, while it increases to 1550 s, as the selectivity is reduced to 11.7.

The comparison between experimental data for air separation with results from simulation studies using the slit potential model can be seen in Fig. 4. The oxygen concentration in the product and nitrogen yield were measured at a constant product flow for different cycle times. A good agreement is observed over a wide range of purities.

Effect of Adsorption Rate Constants

In order to study the combined effect of the adsorption rate constants and purity on the performance of a N_2 PSA unit, a series of simulation runs was carried out at different cycle times. Three cases were considered: in the first case (base case), the original adsorption

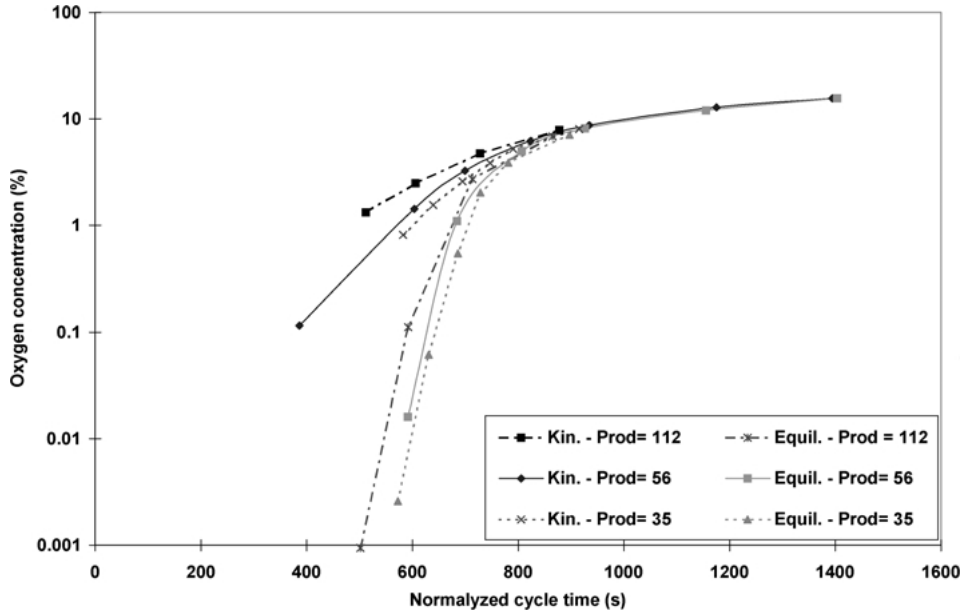

Figure 3. Effect of cycle time on product purity $P = 7.9 \times 10^5$ Pa, $T = 298$ K.

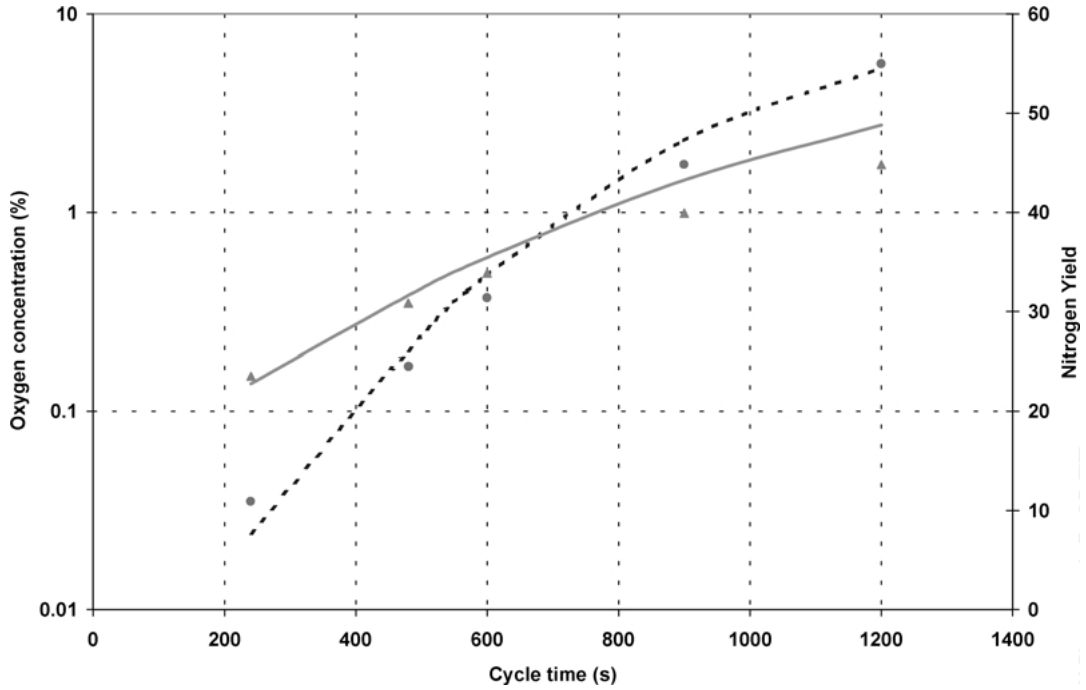

Figure 4. Comparison between experimental and numerical simulation results at different cycle times. $P = 7.9 \times 10^5$ Pa, $T = 298$ K, product flow = 35 Nm^3/h, purge flow = 0.70 Nm^3/cycle, - - - - oxygen, numerical, ● oxygen, experimental, ------ yield, numerical, ▲ yield, experimental.

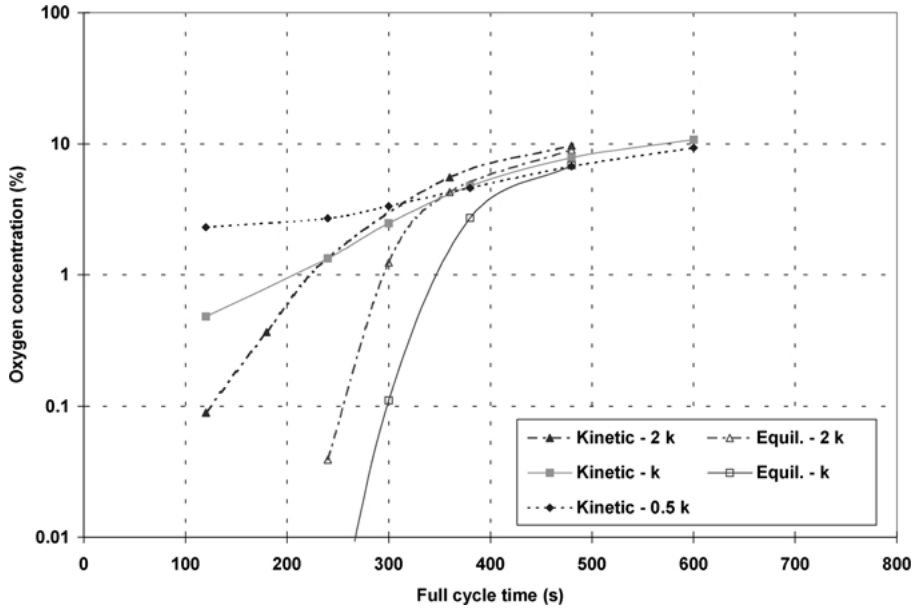

Figure 5. Effect of adsorption/desorption kinetics on product purity $P = 7.9 \times 10^5$ Pa, $T = 298$ K, product flow $= 35$ Nm^3/h.

parameters were used, while in the other two cases, the adsorption rate constants for both N_2 and O_2 were either halved or doubled. In all the cases the selectivity was maintained constant. The observed oxygen concentration is plotted as a function of the cycle time in Fig. 5. It can be seen that, when adsorption equilibrium is assumed for oxygen, higher nitrogen purities are achieved for a slower nitrogen adsorption rate. On the other hand, for the kinetic case, the effect of the adsorption rate depends on the cycle time (or purity). The behavior for long cycle times is, as expected, the same as for the equilibrium case, but for short cycle times (higher purities), the performance improves with the adsorption rates.

This behavior can be explained in terms of the amount of nitrogen adsorbed and its competition with the adsorbed oxygen. For the longer cycle times, the oxygen is close to equilibrium conditions. Therefore, the faster the nitrogen is adsorbed, the more oxygen is displaced leading to a lower product purity. On the other hand, for the shorter cycle times, not only less nitrogen is adsorbed, but also the oxygen adsorption is further away from equilibrium conditions. As the adsorption rate constants increase, more oxygen is adsorbed, and the nitrogen purity increases.

The analysis of the bed concentration profiles provide a better understanding of this behavior. Gas and solid phase concentration profiles at two cycle times and two levels of the adsorption rate constants are represented in Figs. 6–8. The actual conditions for these simulation runs are summarized in Table 1.

The concentration profiles for the production step in Run 1 (long cycle time and fast kinetics) are shown in Fig. 6(a). Due to the fast adsorption rate, the oxygen concentration profiles are relatively steep, and the partial displacement by nitrogen produces the oxygen roll-up. It can also be seen that the initial concentration profile shows an upturn at the exit end of the bed, which is due to the incoming gas from the preceding equalization step, and that the profiles shift by more than half the bed length. The adsorbed nitrogen concentration increases uniformly during the step, displacing the equilibrium adsorbed oxygen. This shift in the concentration profiles are a measure of the amount adsorbed during the step.

The oxygen mole fraction in the gas phase increases almost uniformly during both the equalization (sending bed) and vent steps, and decreases during the purge step to values about half those seen at the end of the production step. The front movement during the equalization (receiving bed) step is shown in Fig. 7(a). The most significant aspect is that a U-shape profile is generated by the incoming gas from the sending bed. During the subsequent pressurization step the profiles shift towards the bed exit.

The concentration profiles for the production step in Run 2 (long cycle time and slow kinetics) are shown in Fig. 6(b). Since nitrogen is adsorbed more slowly

Table 1. Operating conditions for the detailed analysis of the concentration profiles ($P_{ads} = 7.8$ atm, $P_{des} = 1$ atm, product flow $= 112$ Nm^3/h).

	Cycle time (s)	N_2 adsorption rate constant (cm^3/mole s)	O_2 adsorption rate constant (cm^3/mole s)	Change in O_2 concentration (%)	Nitrogen yield change (%)
Base case	360	k_{N_2}	k_{O_2}	–	–
Run 1	360	$2 * k_{N_2}$	$2 * k_{O_2}$	34.5	−8.6
Run 2	360	$0.5 * k_{N_2}$	$0.5 * k_{O_2}$	3.3	10.0
Base case	120	k_{N_2}	k_{O_2}	–	–
Run 3	120	$2 * k_{N_2}$	$2 * k_{O_2}$	−81.5	−16.0
Run 4	120	$0.5 * k_{N_2}$	$0.5 * k_{O_2}$	380	12.1

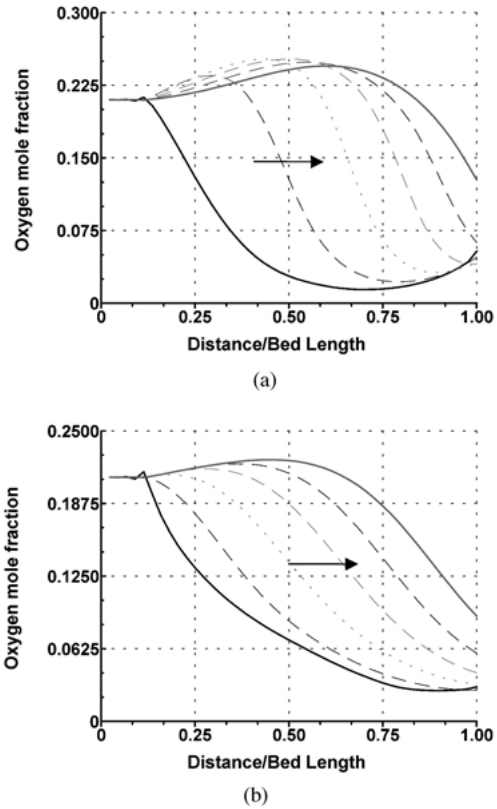

Figure 6. Oxygen concentration profiles during production step. $P_{ads} = 7.8$ atm, $P_{des} = 1$ atm, product flow $= 112$ Nm^3/h, cycle time $= 360$ s, (a) Run 1 ($2 * k_{N_2}$), (b) Run 2 ($0.5 * k_{N_2}$).

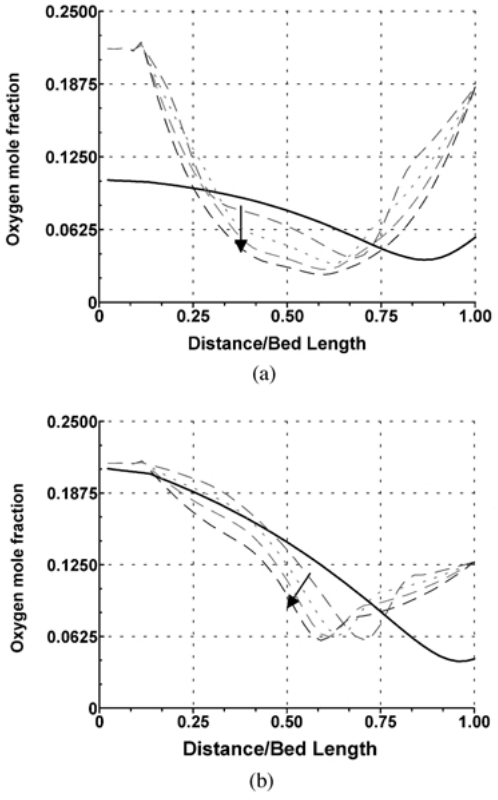

Figure 7. Oxygen concentration profiles during equalization (receiving bed) step. $P_{ads} = 7.8$ atm, $P_{des} = 1$ atm, product flow $=$ 112 Nm^3/h, cycle time $= 360$ s, (a) Run 1 ($2 * k_{N_2}$), (b) Run 2 ($0.5 * k_{N_2}$).

than in the previous case, the oxygen roll-up effect is less pronounced. At the same time, the concentration profiles in both the gas and solid phases are less steep than in the fast kinetics case, and due to the smaller amount of gas adsorbed, the shift during this step is smaller.

At the end of the purge step, the oxygen concentration profiles in both cases have similar shape, but the beds contain less oxygen in Run 1 due to the faster desorption rate. As the equalization step proceeds, and due to the difference in the purity of product gas entering one end of the bed, the concentration profiles

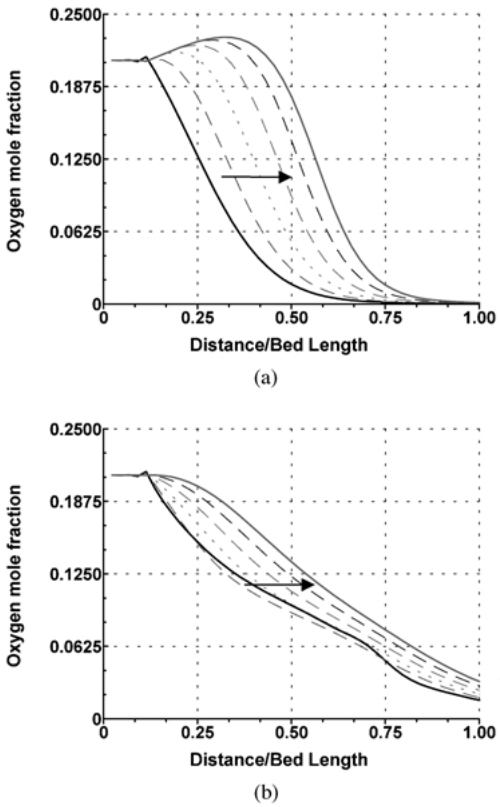

Figure 8. Oxygen concentration profiles during production step. $P_{ads} = 7.8$ atm, $P_{des} = 1$ atm, product flow $= 112$ Nm^3/h, cycle time $= 120$ s, (a) Run 3 $(2 * k_{N_2})$, (b) Run 4 $(0.5 * k_{N_2})$.

during the equalization step are different (Fig. 7(a) and (b)).

In both cases just analyzed, the adsorbed oxygen concentration is almost in equilibrium with the gas phase value, but nitrogen is much less adsorbed in Run 2 than in the first run. Therefore, a higher nitrogen yield, and less amount of adsorbed oxygen displaced (higher nitrogen purity) is observed for the slower kinetic case.

The oxygen concentration profiles during the production step corresponding to Run 3 (short cycle time and fast kinetics) are shown in Fig. 8(a). It can be seen that the movement of the profiles is more restricted than in the previous cases and, due to the fast adsorption rates, a roll-up effect is observed. The oxygen front is relatively sharp, and it only extends over half the bed length.

The concentration profiles during the production step for Run 4 (short cycle time and slow kinetics) are represented in Fig. 8(b). A very different behavior is observed, since no roll-up exists. The oxygen front now extends throughout the whole bed, decreasing almost linearly from the inlet to the exit end of the bed. The nitrogen is adsorbed slowly, and the production time is so short that the increase in the adsorbed nitrogen concentration is very small. In this case, not only less nitrogen is adsorbed than in the faster kinetics case (Run 3), but also less oxygen. Although the yield is higher, the oxygen concentration in the gas phase is also higher, and the nitrogen purity decreases as the adsorption rate decreases.

Conclusions

A simplified analysis has been developed for the nitrogen pressure swing adsorption process over carbon molecular sieves. When operating at long cycle times (low purities), the oxygen can be assumed to have reached equilibrium conditions, and only one rate equation has to be taken into account.

A normalized cycle time was found to be able to lump together all the performance curves, depending only whether equilibrium or kinetic conditions prevail. The nitrogen purity is independent of the productivity, and is only a function of the amount of feed gas entering the bed during one cycle. A good agreement is observed between the numerical simulation and experimental results over a wide range of product purities.

The combined effect of cycle time and adsorption/desorption rate constants is explained in terms of the competitive adsorption of nitrogen and oxygen. For long cycle times, the nitrogen adsorption competes with the oxygen adsorbed on the carbon molecular sieve, and displaces a fraction of it. Therefore, a faster kinetics has a detrimental effect on the nitrogen purity. On the other hand, at short cycle times, the oxygen is not near equilibrium conditions, and a faster kinetics helps achieve a higher nitrogen purity.

Nomenclature

c	Gas phase concentration (mole/m^3)
CT	Full cycle time (s)
D_L	Axial dispersion coefficient (m^2/s)
F	Feed flowrate (m^3/s)
K	Langmuir equilibrium constant (m^3/mole)
K_d	Desorption rate constant (1/s)
k_{sl}	Slit potential rate constant (1/s)
q	Adsorbed phase concentration (mole/m^3)
q_m	Monolayer capacity (mole/m^3)
R	Rate of adsorption (mole/(m^3 s))

t Time (s)
v_z Axial gas velocity (m/s)
Y Yield (dimensionless)
z Axial distance (m)

Greek letters

ε Bed voidage
θ q/q_{m}

Subscripts

i, k Components i, k

References

Farooq, S. and D.M. Ruthven, *Chem. Eng. Sci.*, **46**, 2213–2224 (1991).

LaCava, A.I., J.A. Dominguez, and J. Cardenas, in *Adsorption: Science and Technology*, A.E. Rodrigues, M.D. LeVan, and D. Tondeur (Eds.), NATO ASI Series, Vol. 158, pp. 323–337, 1989a.

LaCava, A.I., V.A. Koss, and D. Wickens, *Gas Sep. Purif.*, **3**, 180–186 (1989b).

LaCava, A.I. and N.O. Lemcoff, *Gas Sep. Purif.*, **10**, 113–115 (1996).

LaCava, A.I. and N.O. Lemcoff, *Hydrocarbon Engineering*, **2**(3), 55–59 (1997).

Lemcoff, N.O., in *Adsorption and its Application in Industry and Environmental Protection*, A. Dabrowski (Ed.), pp. 347–370, Elsevier, Amsterdam, 1999.

Raghavan, N.S. and D.M. Ruthven, *AIChE Journal*, **31**, 2017–2025 (1985).

Ruthven, D.M. and S. Farooq, *Gas Sep. Purif.*, **4**, 141–148 (1990).

Ruthven, D.M., S. Farooq, and K.S. Knaebel, *Pressure Swing Adsorption*, VCH, New York, 1994.

Schork, J.M., R. Srinivasan, and S.R. Auvil, *Ind. Eng. Chem. Research*, **32**, 2226–2235 (1993).

Shirley, A.I. and N.O. Lemcoff, *AIChE Journal*, **43**, 419–424 (1997).

Yang, R.T., *Gas Separation by Adsorption Processes*, Butterworths, Boston, 1987.